University of Bath

Alternative formats
If you require this document in an alternative format, please contact:
openaccess@bath.ac.uk

15% reduction in AC loss of a 3-phase 1 MVA HTS transformer by exploiting asymmetric conductor critical current

Journal of Physics Communications

PAPER

15% reduction in AC loss of a 3-phase 1 MVA HTS transformer by exploiting asymmetric conductor critical current

Zhenan Jiang[1] , Wenjuan Song[2], Xiaoze Pei[2], Jin Fang[3], Rodney A Badcock[1] and Stuart C Wimbush[1]

1 Robinson Research Institute, Victoria University of Wellington, 69 Gracefield Road, Lower Hutt 5011, New Zealand
2 Department of Electronic & Electrical Engineering, The University of Bath, Bath BA2 7AY, United Kingdom
3 School of Electrical Engineering, Beijing Jiaotong University, Beijing 100044, People's Republic of China

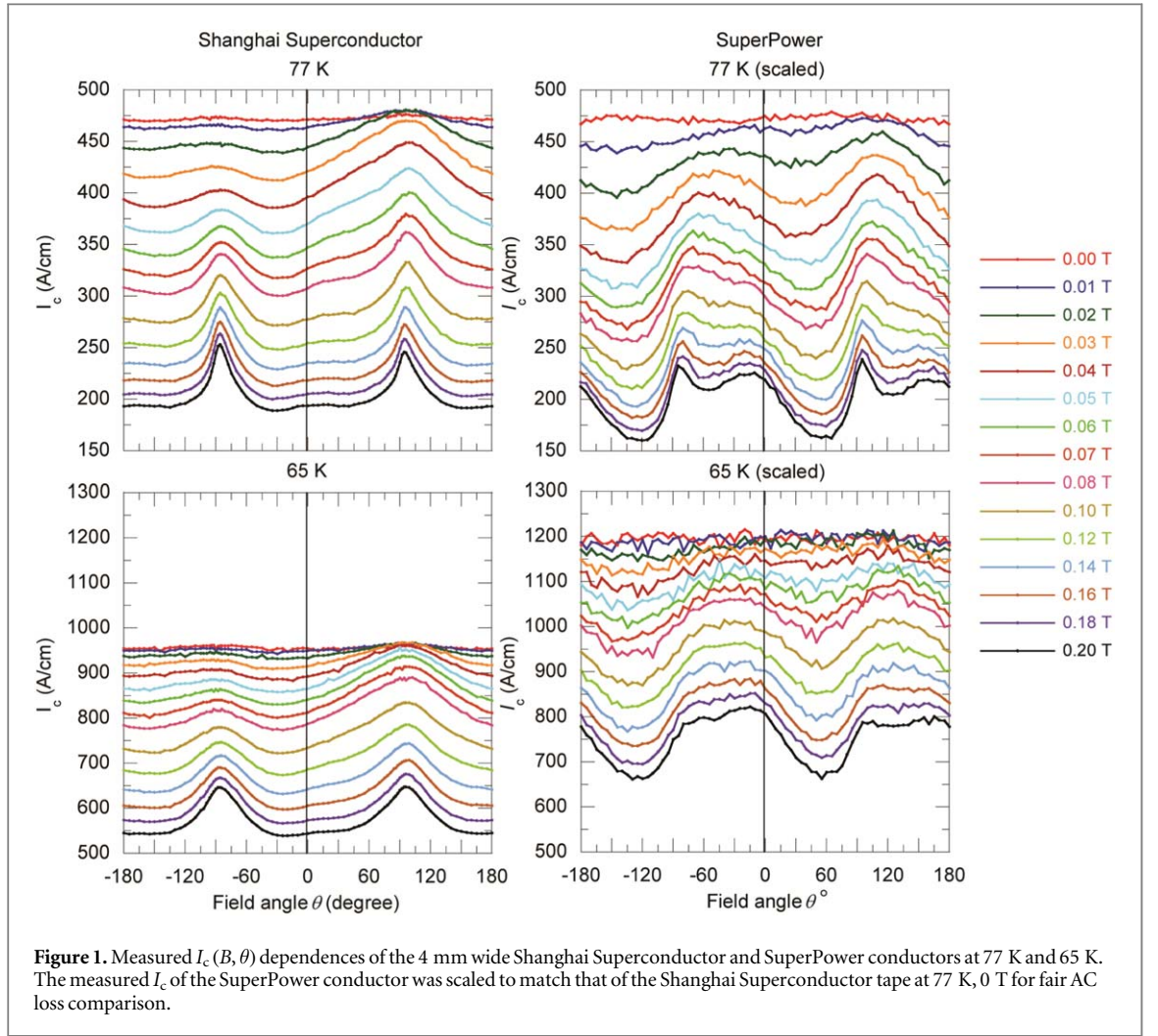E-mail: zhenan.jiang@vuw.ac.nz

Abstract

An asymmetric dependence of the critical current on the direction of an applied magnetic field in HTS coated conductors has a non-trivial influence on the AC loss of coil windings. We report the modelled influence of real conductor critical current asymmetry on the AC loss characteristics of a 1 MVA HTS transformer design previously demonstrated by the Robinson Research Institute as well as a stand-alone coil having the same geometrical and electrical parameters as the low voltage (high current) winding of the transformer. We compare two commercial HTS conductors with distinctive differences in their critical current asymmetry and show a maximum variation of 15% and 29% in the calculated AC loss of the transformer and the stand-alone coil winding, respectively, when the conductor orientation is varied in the top and bottom halves of the windings. AC loss simulation giving consideration to asymmetric conductor critical current before winding the transformer could lead to substantial AC loss reduction even using the same amount of conductor and the same transformer design.

1. Introduction

(RE)Ba$_2$Cu$_3$O$_{7-\delta}$ (REBCO) coated conductors are becoming a prime conductor choice for high temperature superconducting (HTS) transformers [1–10], rotating machines [11], fault current limiters [12–14], and high-field magnets [15]. REBCO conductors generally exhibit asymmetry in their critical current characteristics under applied magnetic fields [16, 17] as a function of magnetic field direction, $I_c(\theta)$, as exemplified in figure 1, where the angle θ is defined as the angle between the normal to the conductor face and the magnetic field in a left-handed system with respect to the direction of current flow as shown in figure 2.

Kubiczek *et al* [18] showed that non-uniform asymmetric $I_c(\theta)$ characteristics of a conductor along the conductor can cause more than 6.7% difference in the I_c value of the conductor. Ainslie *et al* [19] showed that the dynamic resistance in a coated conductor subjected to magnetic fields impinging at different angles exhibits asymmetry due to the asymmetric $I_c(\theta)$ characteristics of the conductor. Zhang *et al* [20] and Hong *et al* [21] showed that coil I_c can be varied by changing the direction of the applied magnetic field relative to the coils due to the asymmetric $I_c(\theta)$ characteristics of the constituent conductors of the coils. More recently, in our previous work, we showed both coil I_c and AC loss in an HTS hybrid winding comprising a stack of six double pancake coils can be substantially altered simply by flipping the orientation of the two end windings [22]. However, there has been no report investigating the influence of $I_c(\theta)$ characteristics on the AC loss of an actual HTS device. Fluctuation in I_c values of a coated conductor along the conductor length may have some impact on both I_c and AC loss in coil windings wound with the conductor. However, it is out of the scope of this paper [23].

We therefore carried out 2D FEM simulations of a 1 MVA HTS transformer wound with two different commercial conductors (Shanghai Superconductor ST1911-89 and SuperPower SCS4050-AP) having different $I_c(B, \theta)$ characteristics at both 77 K and 65 K covering the range of typical operating temperatures of HTS transformers. The transformer geometry and electrical design is the same as that of the 3-phase 1 MVA HTS

Figure 1. Measured I_c (B, θ) dependences of the 4 mm wide Shanghai Superconductor and SuperPower conductors at 77 K and 65 K. The measured I_c of the SuperPower conductor was scaled to match that of the Shanghai Superconductor tape at 77 K, 0 T for fair AC loss comparison.

transformer previously demonstrated at the Robinson Research Institute [2, 6]. The transformer employs fully transposed Roebel cables in the low voltage (LV) windings for dealing with high current and AC loss reduction [24–26]. The coil orientation (and thus the conductor winding direction) was varied in the top and bottom halves of both the high voltage (HV) and the LV windings to investigate the influence of the conductor $I_c(\theta)$ properties on the AC loss of the transformer. In addition, a stand-alone coil having the same geometric and electrical parameters as the LV winding of the transformer was also simulated and the results compared with those for the LV windings of the transformer in order to probe the difference in AC loss dependence of inductive (stand-alone) windings and non-inductive (transformer) windings on $I_c(\theta)$ properties.

2. Numerical methods

The simulation is based on our previously presented method which was validated by comparing the simulated results with the AC loss measurement data on the 1 MVA transformer as well as the result obtained using the minimum magnetic energy variation (MMEV) method [23]. The simulation combines the *H*-formulation and the homogenization method implemented using COMSOL Multiphysics [27–29].

A 2D axisymmetric model was built to calculate the AC loss in the transformer. Radial and axial magnetic fields H_r and H_z, denoted as H $= [H_r, H_z]^\mathrm{T}$, are directly solved in the finite element model. The governing equation, in the form of a partial differential equation, is derived from Maxwell's equations as follows:

$$\nabla \times \boldsymbol{E} = -\partial \boldsymbol{B}/\partial t \tag{1}$$

$$\nabla \times \boldsymbol{H} = \boldsymbol{J} \tag{2}$$

$$\boldsymbol{E} = \rho \boldsymbol{J} \tag{3}$$

$$\boldsymbol{B} = \mu \boldsymbol{H} \tag{4}$$
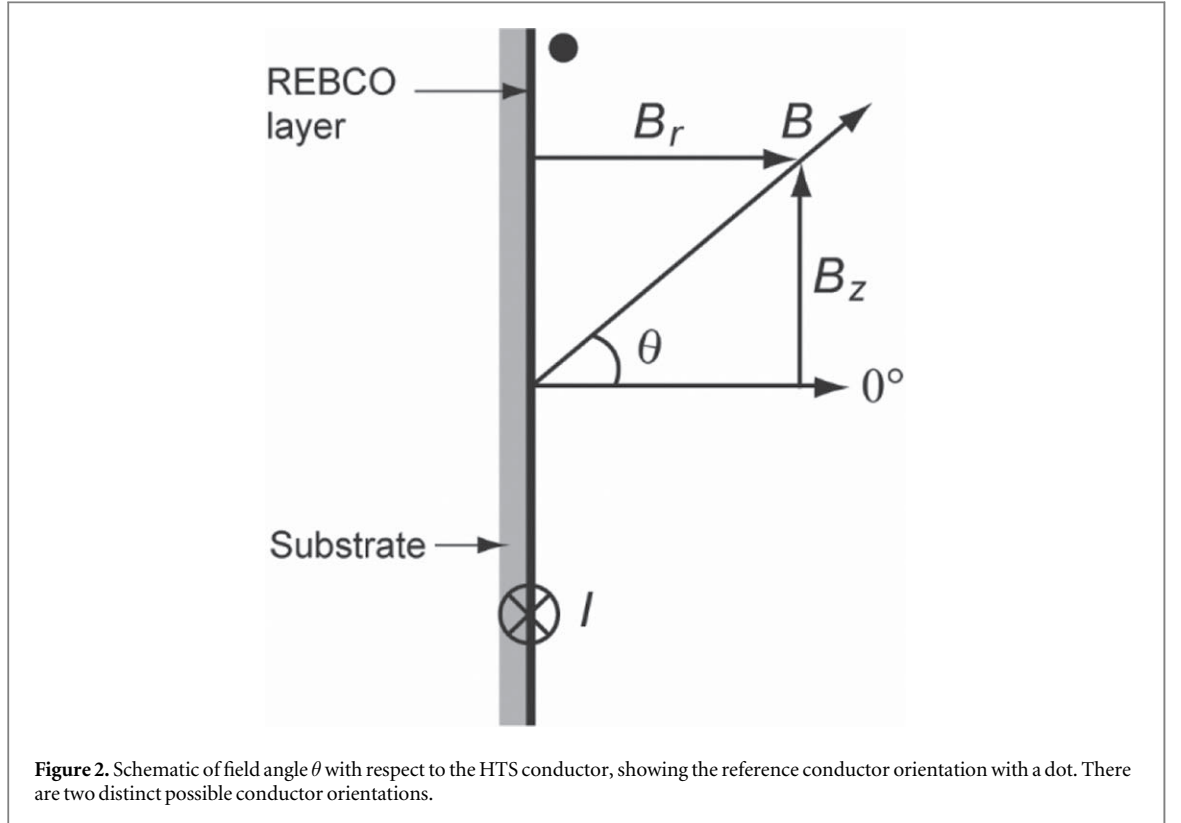
Figure 2. Schematic of field angle θ with respect to the HTS conductor, showing the reference conductor orientation with a dot. There are two distinct possible conductor orientations.

Table 1. Transformer geometry and electrical design.

Winding	HV	LV
Inner diameter (mm)	345	300
Number of turns in axial direction	48	20
Number of turns in radial direction	19	1
Total number of turns	912	20
Conductor width (mm)	4	12.1
Conductor thickness (mm)	0.22	0.8
Axial gap between turns (mm)	2.13	2.1
Number of strands in Roebel cable	—	16
Strand width (mm)	—	5
Gap between Roebel stacks (mm)	—	2.1
Rated current amplitude (A)	42.9	1964

$$\partial(\mu_0\mu_r H)/\partial t + \nabla \times (\rho\nabla \times H) = 0 \tag{5}$$

By substituting the two field variables H_r and H_z into (5), the governing equations can be further derived as,

$$\frac{\partial(\mu_0\mu_{re}H_r)}{\partial t} - \frac{\partial E_\varphi}{\partial z} = 0 \tag{6}$$

$$\frac{\partial(\mu_0\mu_{re}H_z)}{\partial t} + \frac{1}{r}\frac{\partial(rE_\varphi)}{\partial r} = 0 \tag{7}$$

$$E_\varphi = \rho J_\varphi = \rho(\partial H_r/\partial z - \partial H_z/\partial r) \tag{8}$$

where $\mu_0 = 4\pi \times 10^{-7}\,\mathrm{H\,m^{-1}}$ is the vacuum permeability and $\mu_{re} = 1$ is the relative permeability of the transformer windings. ρ is the resistivity of the material. For air we use $\rho_{\mathrm{air}} = 1\,\Omega\mathrm{m}$, while for the superconductor ρ_{HTS} is defined based on the nonlinear E—J power law shown in (9),

$$\rho_{\mathrm{HTS}} = \frac{E_c}{J_c(\boldsymbol{B})}\left|\frac{J_\varphi}{J_c(\boldsymbol{B})}\right|^{(n-1)} \tag{9}$$

where $J_c(\boldsymbol{B})$ is the critical current density as a function of the magnetic field, $E_c = 10^{-4}\,\mathrm{V\,m^{-1}}$ is the electric field criterion used to define the critical current and $n = 25$ is the power-law index of the E—J relationship. n value varies with magnetic field and has some minor impact in simulation results [19]. However, the main purpose of
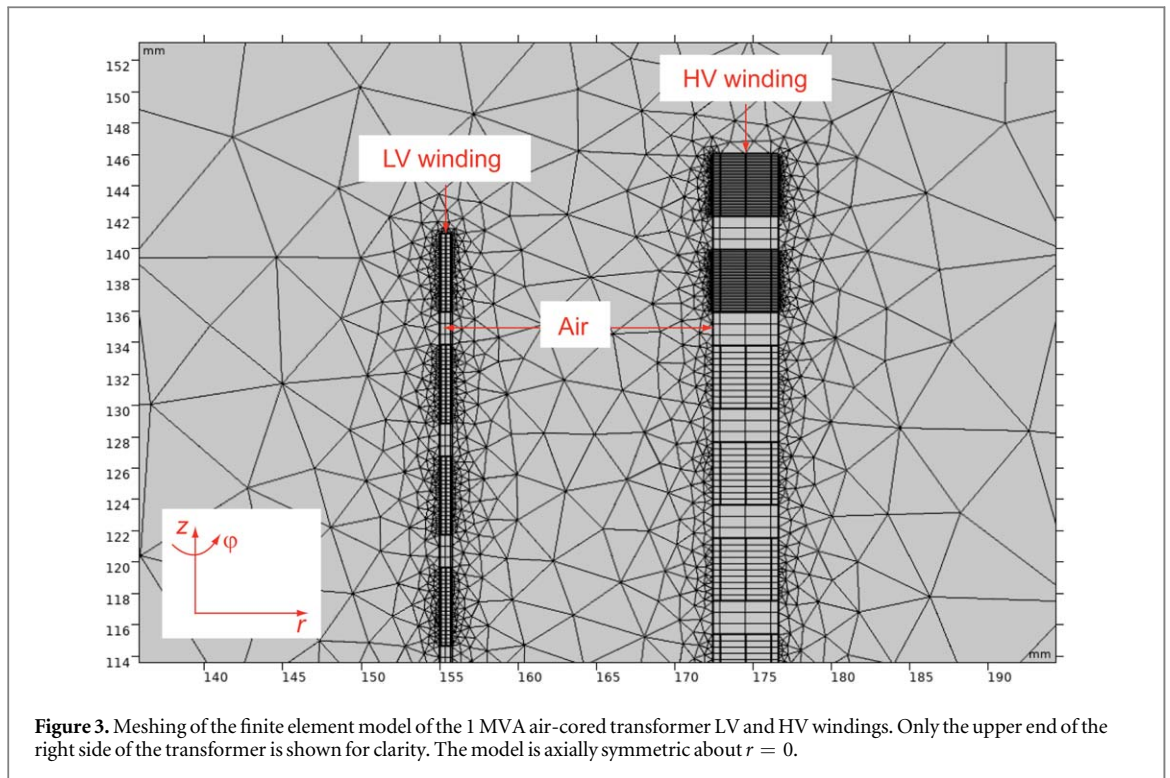
Figure 3. Meshing of the finite element model of the 1 MVA air-cored transformer LV and HV windings. Only the upper end of the right side of the transformer is shown for clarity. The model is axially symmetric about $r = 0$.
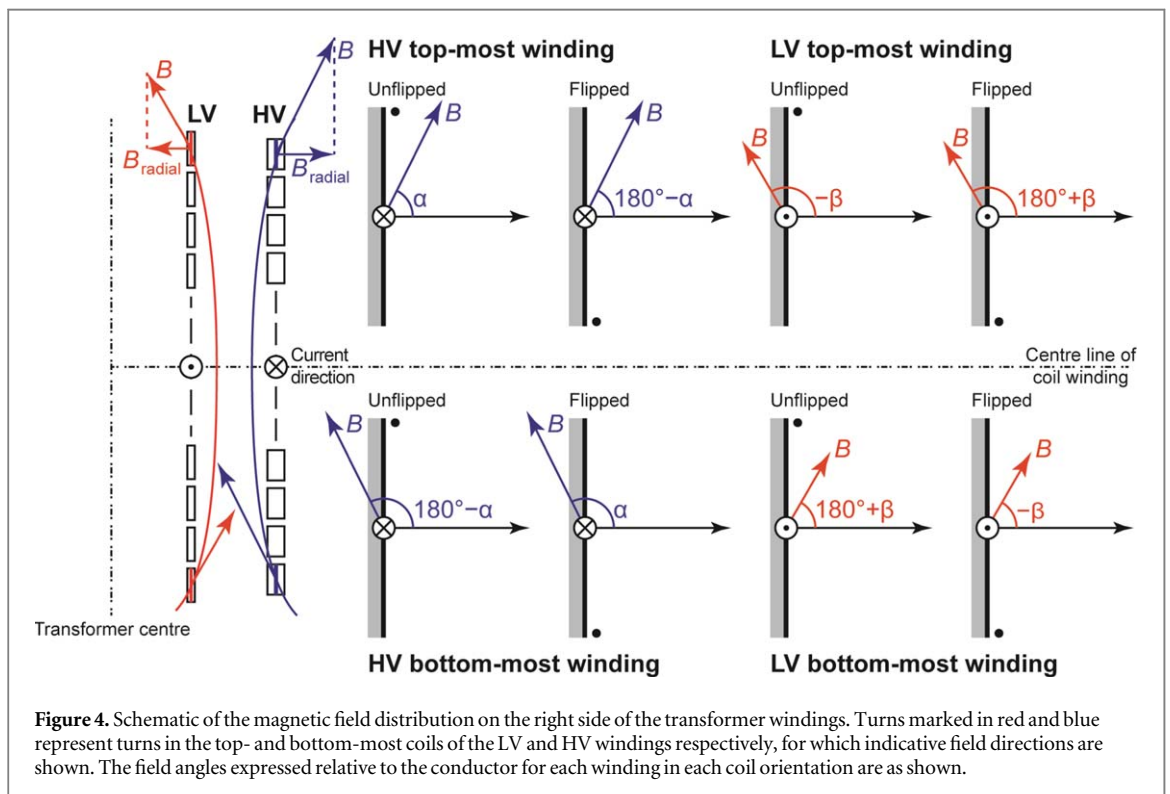
Figure 4. Schematic of the magnetic field distribution on the right side of the transformer windings. Turns marked in red and blue represent turns in the top- and bottom-most coils of the LV and HV windings respectively, for which indicative field directions are shown. The field angles expressed relative to the conductor for each winding in each coil orientation are as shown.

the simulations in the present work is to see the difference of AC loss results in the 1 MVA transformer due to asymmetric $J_c(B, \theta)$ and to test an idea for reducing the AC loss in HTS transformers by applying the same n value for all different configurations. Therefore, only once constant *n* value was used in the present work.

Table 1 describes the geometry and the electrical design of the 1 MVA transformer modelled in the simulation. The HV winding comprises stacks of double pancake coils wound from 4 mm wide conductors while the LV winding is a 20-turn solenoid wound with 16/5 Roebel cable (assembled with sixteen 5 mm wide strands). Roebel cables can be modelled as two parallel stacks of conductors where each conductor carries the same current [30–32]. Therefore, each Roebel turn in the LV winding was modelled as a double pancake coil. In

Table 2. (B_{radial}, B_{axial}) components determined from the field angles in figure 4 for the different HV and LV coil configurations.

	UUUU	LLUU	UULL	LLLL
Top half HV winding	(B_r, B_z)	$(-B_r, B_z)$	(B_r, B_z)	$(-B_r, B_z)$
Bottom half HV winding	$(-B_r, B_z)$	(B_r, B_z)	$(-B_r, B_z)$	(B_r, B_z)
Top half LV winding	$(B_r, -B_z)$	$(B_r, -B_z)$	$(-B_r, -B_z)$	$(-B_r, -B_z)$
Bottom half LV winding	$(-B_r, -B_z)$	$(-B_r, -B_z)$	$(B_r, -B_z)$	$(B_r, -B_z)$

reality, the strands in a Roebel cable are not perfectly aligned, and hence it might result in some changes in cable I_c and AC loss values [33].

Figure 3 shows the meshing of the upper end of the 1 MVA transformer. Fine meshes of 40 elements were used in the axial direction for the end of both LV and HV windings, while coarser meshes of 20 and 10 elements were used in the middle of the LV and HV windings, respectively. This is based on the fact that larger AC loss is generated at the ends of the coil windings due to the larger radial magnetic field component while less AC loss is generated in the middle because the magnetic field lies mainly parallel to the face of the HTS conductor in this region. Structured meshes were introduced in the air regions between the superconducting coils within each winding, and triangular meshing was used in the broader air region between the windings [34].

Figure 4 shows a schematic cross-section of the right side of the transformer winding. In spite of the non-inductive nature of the transformer winding whereby conductors in the LV and HV windings carry current in opposing directions, the resultant magnetic field distribution is more or less as shown in the schematic, i.e. conductors at the ends of the windings are exposed to a greater radial (perpendicular) magnetic field component than those in the centre although the directions of the radial (perpendicular) magnetic field components are opposite in the LV and HV windings.

We consider a single turn in the top-most coil of the HV winding as marked in blue on the figure. If we define the upper edge of the coil as a reference for the conductor orientation, then the field angle relative to the conductor is α. When the coil is flipped upside down, from the perspective of the conductor this has the effect of inverting the field angle and offsetting it by 180°; in other words the field angle now becomes $180° - \alpha$. If we instead consider a single turn in the bottom-most coil of the HV winding with its conductor reference orientation at the upper edge, then by symmetry the field angle is also $180° - \alpha$, and when that coil is flipped the field angle becomes α. In the case of the LV windings, due to the reversed direction of current flow compared to the HV winding, which has an effect equivalent to reversing the field direction relative to the conductor, or again of offsetting the field angle by 180°, the bottom-most winding in an unflipped configuration has a field angle relative to the conductor of $180° + \beta$, flipping the coil orientation yields a field angle of—β, while in the top-most winding the corresponding field angles are—β and $180° + \beta$.

If we consider HV and LV winding combinations with their top and bottom halves having different coil orientations, then there will be 16 possible configurations. We can define a coil configuration where the upper edge (U) of the coils of both the top and bottom halves of the HV and LV windings is the reference orientation as UUUU and a winding combination where the lower edge (L) of the coils of both the top and bottom halves of the HV and LV windings is the reference orientation as LLLL. In this four-character notation, the first two characters denote the conductor orientation of the top and bottom halves of the HV winding while the last two characters denote the conductor orientation of the top and bottom halves of the LV winding. In this way, we can define the full set of possible coil configurations. However, in this study, we only focus on the four configurations having the same coil orientation within each (LV or HV) winding: UUUU, LLUU, UULL, and LLLL.

In the AC loss simulation, we use a three-column look-up table [B_{radial}, B_{axial}, J_c (B_{radial}, B_{axial})], where B_{radial} and B_{axial} are the radial and axial components of the magnetic field, and J_c (B_{radial}, B_{axial}) is the critical current density derived from the measured I_c (B, θ) curves of figure 1 by dividing by the cross-sectional area of the superconductor layer using the direct interpolation method [35]. If the field angle is θ then $B_{radial} = B\cos(\theta) = B_r$ and $B_{axial} = B\sin(\theta) = B_z$, while if the field angle is $180°-\theta$ then $B_{radial} = B\cos(180°-\theta) = -B_r$ and $B_{axial} = B\sin(180°-\theta) = B_z$. Table 2 lists the B_{radial} and B_{axial} components for the UUUU, LLUU, UULL and LLLL configurations.

In the simulation, the I_c of the SuperPower conductors at 77 K was scaled to that of the Shanghai Superconductor tape at 77 K to allow fair comparison by multiplying a coefficient, which is the ratio of the self-field I_c of Shanghai Superconductor tape at 77 K and that of SuperPower conductor at 77 K. The coefficient was also multiplied to the measured I_c (B, θ) curves of the SuperPower conductor at 65 K. The scaled I_c (B, θ) curves of the SuperPower conductor at 77 K and 65 K can be seen in figure 1.

3. Simulation results and discussion

Tables 3 and 4 list the simulation results for each coil configuration wound with each type of conductor at 77 K and 65 K at different LV winding current amplitudes, $I_{t, LV}$. The results for UUUU and LLUU wound with Shanghai Superconductor tape broadly agree with one another at both temperatures, as do the results for UULL and LLLL. The results for SuperPower conductor are similar, but not quite so closely-matched. In the tables, we see a difference between the two configurations at both 77 K and 65 K. This difference is made clearer on figure 5, from which it is apparent that the difference of Shanghai Superconductor tape at both 77 K and 65 K is much smaller than that of SuperPower conductor. At the rated current of 1964 A, the difference is 0.7% at 77 K and 1.9% at 65 K for the Shanghai Superconductor tape, compared to 10.7% and 15.6% at both temperatures for the SuperPower conductor.

If we compare the $I_c(B, \theta)$ curves for the different conductors (figure 1), we see that the Shanghai Superconductor tape has a relatively symmetric I_c about the *ab*-peak at $\theta = \pm 90°$ but shows a large difference in I_c when the field is reversed (i.e. at θ and $\theta - 180°$). In contrast, the SuperPower conductor combines both a highly asymmetric I_c about the *ab*-peak and upon field reversal. Furthermore, the difference in I_c upon reversing the field is most pronounced (for both conductors) at low fields, less than about 0.1 T, while the asymmetric I_c about the *ab*-peak in the SuperPower conductor extends clearly up to and beyond 0.2 T, the field calculated to be incident on the end coils of the transformer winding. As we have shown (figure 4), the effect of reversing the coils is to change the incident field angle from $+ \theta$ to $180° - \theta$, or from $180° - \theta$ to θ. Both the top and bottom halves of the HV and LV windings of the UUUU configuration are reversed when changing to the LLLL configuration. Therefore, the difference between the AC loss values of the UUUU and LLLL configurations arises from the asymmetry of $I_c(B, \theta)$ within each half-cycle of figure 1. This asymmetry is far greater for the SuperPower conductor at both temperatures, and hence the difference in AC loss between the UUUU and LLLL configurations is generally greater for the SuperPower conductor than the Shanghai Superconductor tape. The reason for the agreement between the AC loss values for the UUUU and LLUU (or UULL and LLLL) configurations wound with Shanghai Superconductor tape is mainly due to the dominance of the LV windings in determining the overall AC loss. For example, AC loss values in the UUUU configuration at the rated current in the LV and HV windings are 81.4 W and 7.0 W, respectively. In UUUU and LLUU (or UULL and LLLL) configurations, the top and bottom halves of the LV windings share the same conductor orientation while the top and bottom halves of the HV windings have opposite conductor orientation. The opposite conductor orientation in the HV windings should cause some difference in the AC loss in the HV windings. However, the magnetic field around the end coil of the HV winding varies between 0.09 T to 0.18 T, at which fields the symmetry of $I_c(B, \theta)$ between each half-cycle for the Shanghai Superconductor tape is not perfect but rather good. Therefore, as a result, the UUUU and LLUU (or UULL and LLLL) configurations have almost the same AC loss. In contrast, there is a slight difference in the AC loss values in these configurations wound with the SuperPower conductor at both 77 K and 65 K. We attribute this difference to the relatively poor asymmetry of $I_c(B, \theta)$ between each half-cycle of the SuperPower conductor. The $I_c(B, \theta)$ data also explains the temperature dependence of the AC loss difference. In the case of the Shanghai Superconductor tape, at 65 K and moderate fields, there is a marginally higher degree of asymmetry within each half-cycle of the $I_c(B, \theta)$ curves than at 77 K, contributing to an increased difference in AC loss.

Figure 6 highlights the comparison of the simulated AC loss results for UUUU and LLLL coil configurations wound from SuperPower conductor at different temperatures. The AC loss at 77 K is 16 to 25 times larger than that at 65 K for the coil configurations. This result is consistent with the AC loss measurement and simulation results where AC loss is found to increase as the 3rd to 4th power of the I_t/I_c ratio. Therefore, the results should be due to the increased I_c of the conductor at 65 K compared to 77 K as reported in hybrid HTS coil windings [6, 36]. However, this may only be true when the HTS coils generate a low perpendicular magnetic field component in the end windings of the coils. In the case where an HTS coil generates large radial (perpendicular) magnetic field components in the end windings, the AC loss in the coil is dominated by magnetization loss in the end windings. Because magnetisation loss is proportional to critical current density when the radial magnetic field component is larger than the penetration field, an increased I_c at lower temperatures will lead to an increase (rather than a decrease) in the AC loss in the coil [37, 38].

It is worth emphasising that this significant (around 16%) variation in AC loss is created simply by reversing the orientation of the conductor in the windings. This implies that just by controlling the conductor orientation during winding of the transformer, we can achieve a substantial reduction in the overall AC loss of the transformer. For example, a total of approximately 54.8 W of AC loss reduction can be achieved for the 1 MVA transformer wound with SuperPower conductor operating at the rated current at 77 K. This is without considering the cooling penalty which ranges between 15 and 20 at 77 K.

Figure 7 compares the simulated AC loss results in UUUU configurations for the different conductors at 77 K. The AC loss values for SuperPower conductor are substantially larger than those for Shanghai
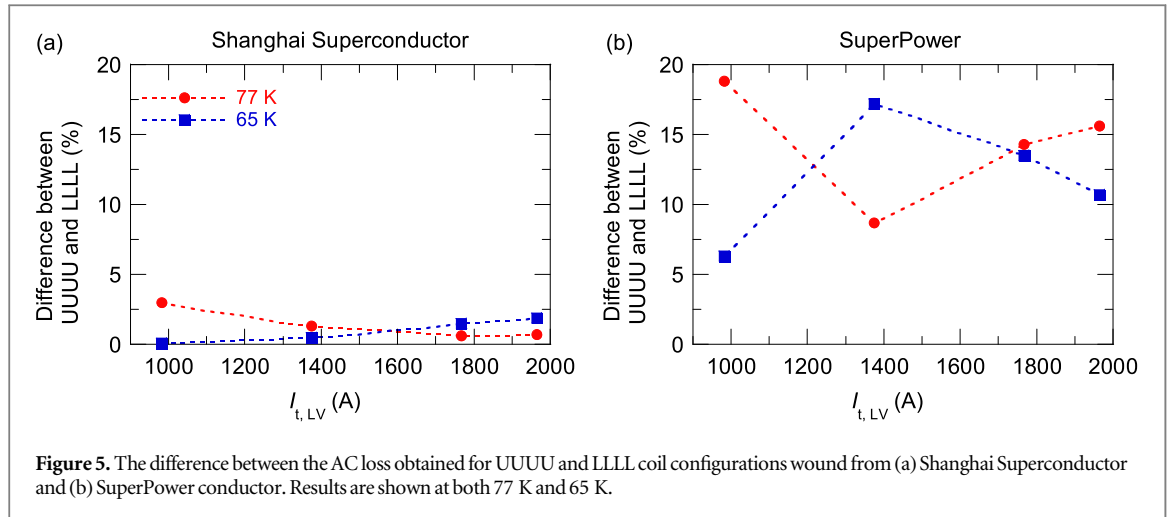
Figure 5. The difference between the AC loss obtained for UUUU and LLLL coil configurations wound from (a) Shanghai Superconductor and (b) SuperPower conductor. Results are shown at both 77 K and 65 K.

Table 3. Simulated AC loss per phase results for the 1 MVA transformer wound with Shanghai Superconductor tape.

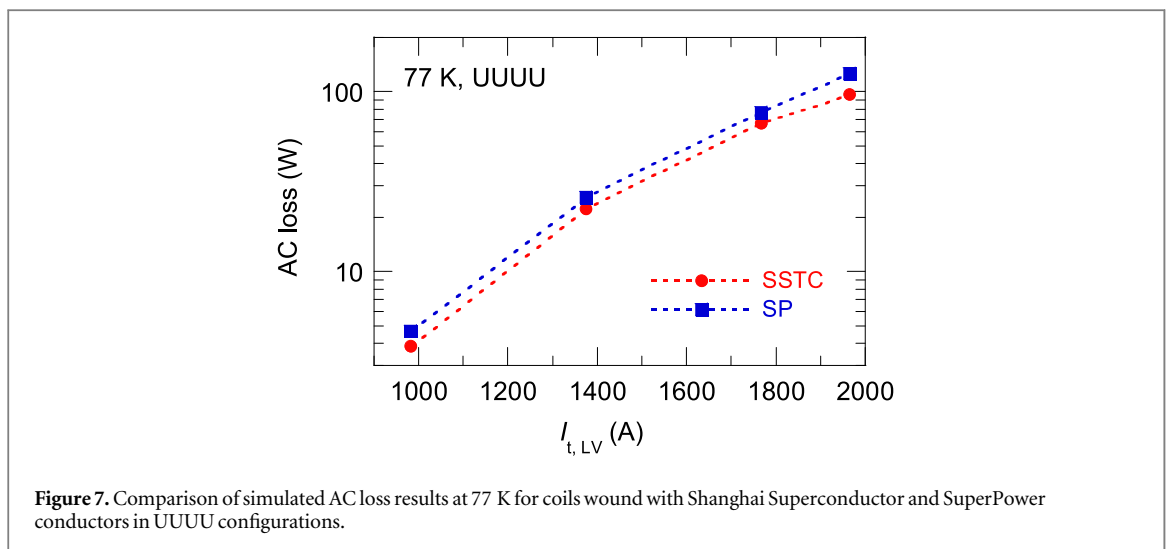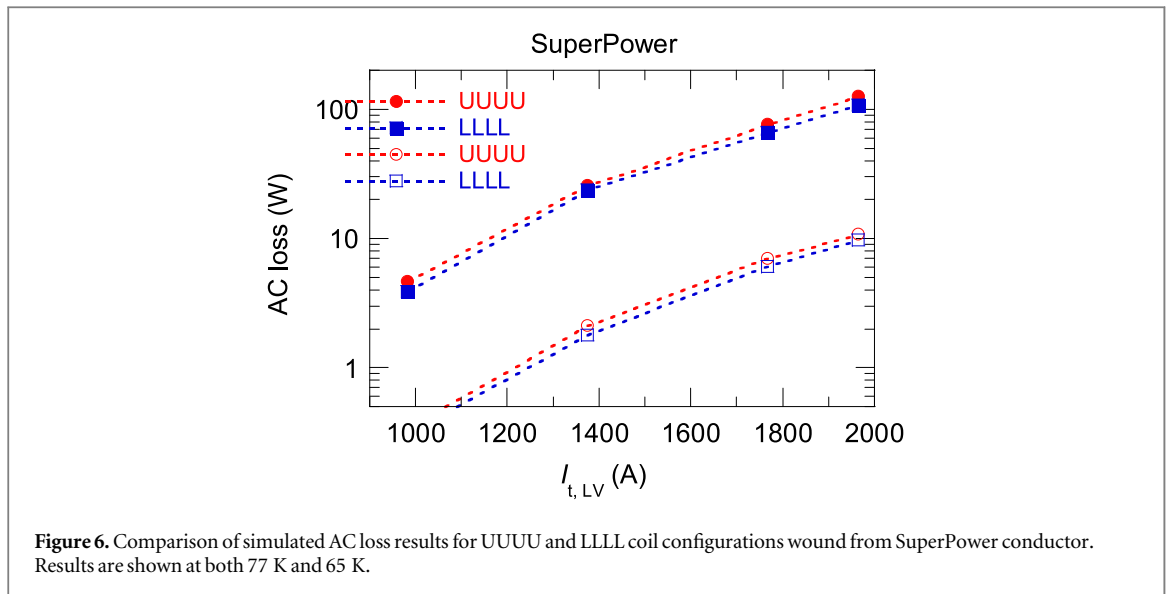|		Coil current $I_{t, LV}$ (A)		AC loss per phase (W)				Difference between UUUU and LLLL (%)
				UUUU	LLUU	UULL	LLLL	
Shanghai Superconductor	77 K	$0.5\,I_{rated}$	982	3.84	3.84	3.96	3.96	3.0
		$0.7\,I_{rated}$	1375	22.36	22.36	22.66	22.66	1.3
		$0.9\,I_{rated}$	1768	66.81	66.76	66.45	66.40	0.6
		I_{rated}	1964	97.01	96.87	96.41	96.29	0.7
	65 K	$0.5\,I_{rated}$	982	0.37	0.36	0.37	0.37	0.1
		$0.7\,I_{rated}$	1375	2.90	2.89	2.92	2.91	0.5
		$0.9\,I_{rated}$	1768	9.59	9.59	9.73	9.74	1.5
		I_{rated}	1964	14.30	14.32	14.57	14.58	1.9

Table 4. Simulated AC loss per phase results for the 1 MVA transformer wound with SuperPower conductor.

		Coil current $I_{t, LV}$ (A)		AC loss per phase (W)				Difference between UUUU and LLLL (%)
				UUUU	LLUU	UULL	LLLL	
SuperPower	77 K	$0.5\,I_{rated}$	982	4.66	4.59	3.93	3.86	18.8
		$0.7\,I_{rated}$	1375	25.81	25.55	23.93	23.67	8.7
		$0.9\,I_{rated}$	1768	77.00	76.01	67.72	66.70	14.3
		I_{rated}	1964	126.35	124.38	110.14	108.10	15.6
	65 K	$0.5\,I_{rated}$	982	0.159	0.159	0.158	0.158	6.3
		$0.7\,I_{rated}$	1375	1.397	1.397	1.115	1.115	17.2
		$0.9\,I_{rated}$	1768	5.334	5.335	4.582	4.583	13.5
		I_{rated}	1964	8.449	8.450	7.493	7.494	10.7

Superconductor. This can be explained by the difference in the I_c of the two conductors at 77 K. Because the self-field I_c values of the conductors were scaled to match, there exists a wide angular region where the I_c values of the SuperPower conductor are much smaller than those of the Shanghai Superconductor tape for a given magnetic field in the range of interest. These lower I_c values will cause larger AC loss for the SuperPower conductor.

Figure 8 compares the $|J/J_c|$ distributions in the end coil (half of the Roebel winding) of the LV winding of LLLL and UUUU configurations wound with SuperPower conductors at 77 K at the rated current. The UUUU (inferior) configuration wound with SuperPower conductor exhibits a larger region of $|J/J_c| > 1$ than the LLLL (superior) configuration. AC loss is mostly generated in regions where $|J/J_c| > 1$, so these results match the observations highlighted in figure 6.

Figure 9 compares the normalised loss distribution at 77 K in each disc of the LV winding of the (inferior) UUUU configuration and a stand-alone solenoid winding with UU configuration which has the same dimensions as well as electrical parameters as the LV winding. Most of the discs in the stand-alone winding have greater loss than the equivalent discs of the LV winding of the transformer except the very middle discs. The difference arises from the

Figure 6. Comparison of simulated AC loss results for UUUU and LLLL coil configurations wound from SuperPower conductor. Results are shown at both 77 K and 65 K.

Figure 7. Comparison of simulated AC loss results at 77 K for coils wound with Shanghai Superconductor and SuperPower conductors in UUUU configurations.

difference of coil winding type: a transformer is broadly a non-inductive winding while the stand-alone winding is an inductive winding. Cancellation of magnetic field occurs in the non-inductive windings and this leads to lower AC loss compared to the equivalent inductive winding. In both coil windings AC loss is mostly generated in the end coils [24, 27, 39]. However, only four discs at each end of the LV winding of the transformer have more loss than the middle discs while the stand-alone winding has 14 end discs having more loss than the middle discs. Therefore, the difference between the LLLL and UUUU coil configurations should be due to AC loss differences in the very end coils of the windings. $I_c(B, \theta)$ asymmetry might have a different impact on the AC loss of different winding types. Therefore, the AC loss in UU and LL configurations of the stand-alone winding wound with Shanghai Superconductor and SuperPower conductors was simulated and compared.

Tables 5 and 6 compare the simulated AC loss results at different currents for stand-alone windings wound with Shanghai Superconductor and SuperPower conductor in UU and LL configurations at 77 K and 65 K. In both cases, there is a difference between the AC loss values in the two configurations. Figure 10 plots these differences. However, the difference is much smaller for Shanghai Superconductor tape and it is much greater for SuperPower conductor. At the rated current, the AC loss difference between the UU and LL configurations at 77 K is as high as 29.4% which is approximately twice the AC loss difference between the UUUU and LLLL configurations in the transformer. This implies that $I_c(B, \theta)$ asymmetry has a greater impact on the AC loss of inductive windings than non-inductive windings. We attribute this difference to the difference in loss distribution profile of the two types of coil windings shown in figure 9.

The same idea can be applied in much larger HTS transformers. Taking an example in a 110 kV/11 kV 3-phase 40 MVA transformer in [24], the rated current for HV and LV winding is 121 Arms and 2100 Arms, respectively. Considering 65 K as operating temperature, HV windings can be composed of stacks of double

Figure 8. Comparison of the $|J/J_c|$ distribution in the end coil of the LV winding for the (a) LLLL, and (b) UUUU configurations wound with SuperPower conductor at rated current at 77 K.
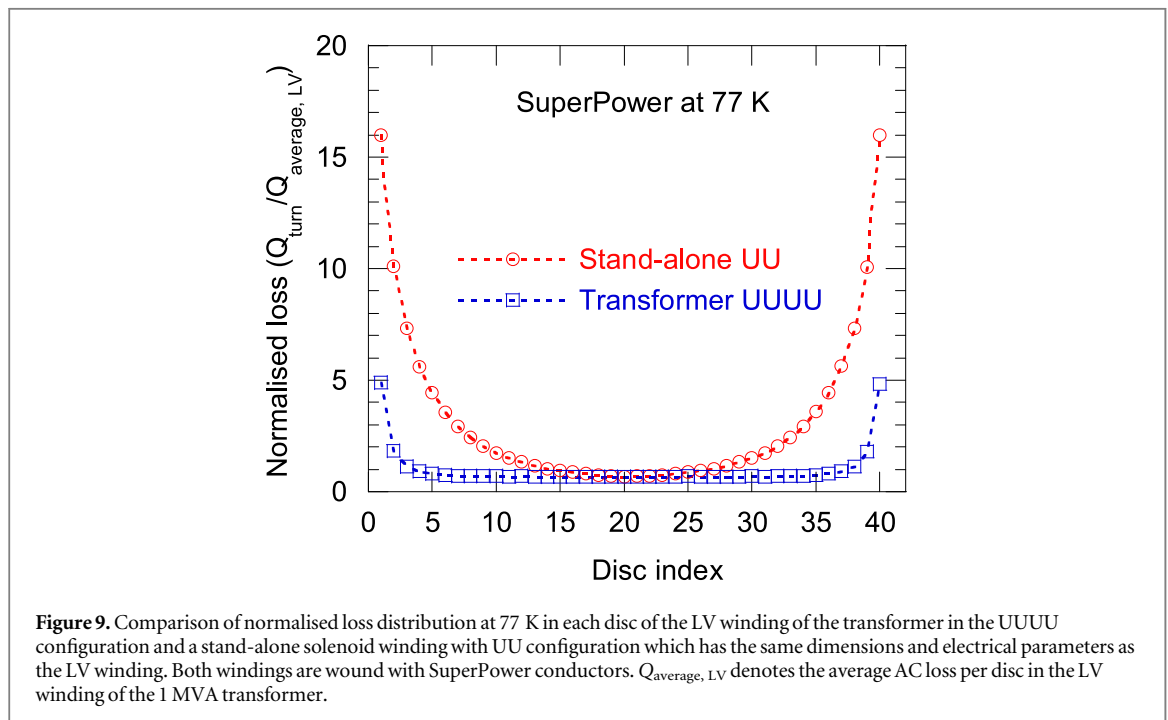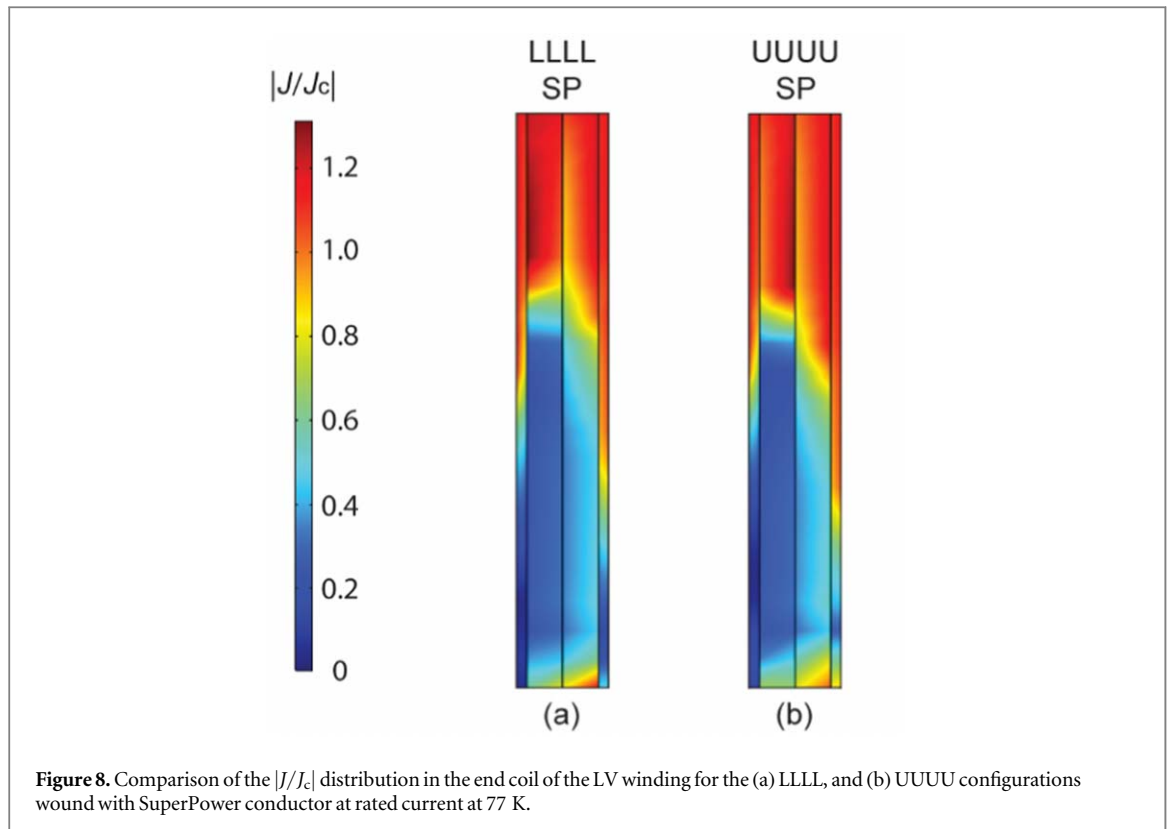

Figure 9. Comparison of normalised loss distribution at 77 K in each disc of the LV winding of the transformer in the UUUU configuration and a stand-alone solenoid winding with UU configuration which has the same dimensions and electrical parameters as the LV winding. Both windings are wound with SuperPower conductors. $Q_{average, LV}$ denotes the average AC loss per disc in the LV winding of the 1 MVA transformer.

pancake coils wound with single coated conductors because I_c of a current lab-scale 4 mm—wide single coated conductor at 65 K and 0.2 T perpendicular magnetic field can exceed 300 A which is much greater than the rated current of the HV winding (171 Apeak) [10]. The rated current for LV winding is 2970 Apeak, and a fifteen 5 mm strand Roebel cable can cope with the rated current, because I_c of the roebel cable could exceed 5500 A at 65 K and 0.2 T perpendicular magnetic field. The winding type of the LV windings is likely to be solenoid winding. To implement the idea, the Roebel cables need to have splicing of punched Roebel strands near the mid-point of the cable before cabling in order to reduce joint numbers. We do not see any substantial difficulties in implementing this idea in practice. At present, no-one does it because the effect is not widely known. Once manufacturers are aware that they can reduce AC loss by 15% simply by taking care of their spool orientation while winding for HV
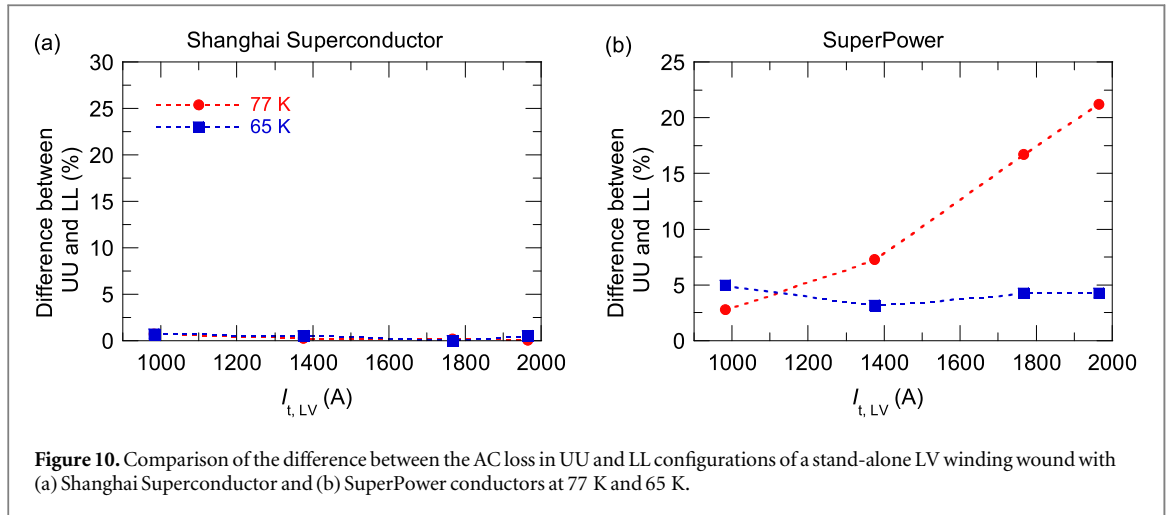
Figure 10. Comparison of the difference between the AC loss in UU and LL configurations of a stand-alone LV winding wound with (a) Shanghai Superconductor and (b) SuperPower conductors at 77 K and 65 K.

Table 5. Simulated AC loss results for the stand-alone winding wound with Shanghai Superconductor tape.

				AC loss per phase (W)		
		Coil current $I_{t, LV}$ (A)		UU	LL	Difference between UU and LL (%)
Shanghai Superconductor	77 K	$0.5\,I_{rated}$	982	20.7	20.9	0.7
		$0.7\,I_{rated}$	1375	67.8	67.9	0.3
		$0.9\,I_{rated}$	1768	159.8	157.6	0.2
		I_{rated}	1964	230.4	226.0	0.1
	65 K	$0.5\,I_{rated}$	982	7.5	7.5	0.7
		$0.7\,I_{rated}$	1375	20.2	20.1	0.3
		$0.9\,I_{rated}$	1768	48.6	48.6	0.2
		I_{rated}	1964	70.4	70.8	0.1

Table 6. Simulated AC loss results for the stand-alone winding wound with SuperPower tape.

				AC loss per phase (W)		
		Coil current $I_{t, LV}$ (A)		UU	LL	Difference between UU and LL (%)
SuperPower	77 K	$0.5\,I_{rated}$	982	23.9	21.7	9.6
		$0.7\,I_{rated}$	1375	84.5	73.8	13.6
		$0.9\,I_{rated}$	1768	238.9	187.2	24.2
		I_{rated}	1964	379.2	281.9	29.4
	65 K	$0.5\,I_{rated}$	982	4.8	4.5	6.4
		$0.7\,I_{rated}$	1375	15.3	14.9	3.0
		$0.9\,I_{rated}$	1768	35.1	33.1	5.9
		I_{rated}	1964	52.0	48.5	7.0

windings and splicing Roebel strands before cable assembly. In terms of reducing cost further, hybrid winding structure can be introduced, i.e. we can use lower I_c conductors in the central part of the windings and high I_c conductors in the end part of the windings [36, 40]. The idea of hybrid winding structure arises from the fact that conductors in the central part of the winding are experiencing parallel magnetic fields and conductors in the end part of the winding are exposed to perpendicular magnetic field. Introducing this idea, we can only need to control the orientation of conductors in the end part of the windings [22].

4. Conclusion

We have numerically investigated the influence of $I_c(\theta)$ asymmetry on the AC loss of an existing HTS 1 MVA transformer as well as a stand-alone coil having the same geometrical and electrical parameters as the low voltage

transformer winding using actual $I_c(B, \theta)$ data obtained from conductors supplied by Shanghai Superconductor and SuperPower.

We observed a substantial difference in the calculated overall AC loss in the HTS transformer when the orientation of the coils (and therefore the conductor) in the top and bottom halves of the windings was varied. A maximum difference at 77 K of 0.7% (Shanghai Superconductor) and 15.6% (SuperPower) was observed for different coil configurations. The result implies that a substantial AC loss reduction is possible in HTS transformers simply by controlling the orientation of the conductor during coil winding. The difference in the AC loss arises from the $I_c(B, \theta)$ asymmetry of the conductors and it appears that local $I_c(B, \theta)$ asymmetry within each half-cycle has a great influence on AC loss.

The stand-alone coil where the orientation of the conductor in the top and bottom halves of the windings was varied gave a maximum 29.4% difference in the simulated AC loss results at 77 K which is far greater than that for the transformer due to the difference in loss distribution profiles of the two types of winding.

The results obtained have important implications for the ultimate efficiency achievable in HTS transformer applications, and therefore the economic viability of the devices. The conclusion obtained in the work can also be extended to many other HTS applications such as NMR (nuclear magnetic resonance), MRI (magnetic resonance imaging), fast ramping and high magnetic field fusion magnets, rotating machines, SMES (superconducting magnetic energy storage), and SFCL (superconducting fault current limiter).

Acknowledgments

Data availability statement

All data that support the findings of this study are included within the article (and any supplementary files).

ORCID iDs

Zhenan Jiang ● https://orcid.org/0000-0002-3482-3510
Rodney A Badcock ● https://orcid.org/0000-0003-0219-9570
Stuart C Wimbush ● https://orcid.org/0000-0003-1636-643X

References

[1] Iwakuma M *et al* 2015 Development of a 3 ϕ-66/6.9 kV-2 MVA REBCO Superconducting Transformer *IEEE Trans. Appl. Supercond.* **25** 5500206
[2] Glasson N D, Staines M P, Jiang Z and Allpress N S 2013 Verification testing for a 1 MVA 3-phase demonstration transformer using 2G-HTS roebel cable *IEEE Trans. Appl. Supercond.* **23** 5500206
[3] Wang Y *et al* 2007 Development of a 630 kVA three-phase HTS transformer with amorphous alloy cores *IEEE Trans. Appl. Supercond.* **17** 2051–4
[4] Hellmann S, Abplanalp M, Elschner S, Kudymow A and Noe M 2019 Current limitation experiments on a 1 MVA-class superconducting current limiting transformer *IEEE Trans. Appl. Supercond.* **29** 5501706
[5] Vysotsky V S *et al* 2017 Development and test results of HTS windings for superconducting transformer with 1 MVA rated power *IEEE Trans. Appl. Supercond.* **27** 5500105
[6] Staines M, Jiang Z, Glasson N, Buckley R G and Pannu M 2015 *High-Temperature Superconducting (HTS) transformers for Power Grid Applications Superconductor in the Power Grid: Materials and Applications* (Cambridge: Woodhead) ch 12 367–97
[7] Hu D, Li Z, Hong Z and Jin Z 2017 Development of a single-phase 330 kVA HTS transformer using GdBCO tapes *Phys. C Supercond.* **539** 8–12
[8] Dai S, Ma T, Qiu Q, Zhu Z, Teng Y and Hu L 2016 Development of a 1250 kVA superconducting transformer and its demonstration at the superconducting substation *IEEE Trans. Appl. Supercond.* **26** 5500107
[9] Yazdani-Asrami M, Staines M, Sidorov G and Eicher A 2020 Heat transfer and recovery performance enhancement of metal and superconducting tapes under high current pulses for improving fault current-limiting behavior of HTS transformers *Supercond. Sci. Technol.* **33** 095014
[10] Song W, Jiang Z, Staines M, Badcock R A, Wimbush S C, Fang J and Zhang J 2020 Design of a single-phase 6.5 MVA/25 kV superconducting traction transformer for the Chinese Fuxing high-speed train *Int. J. Electr. Power Energy Syst.* **119** 105956
[11] Haran K S *et al* 2017 High power density superconducting rotating machines—development status and technology roadmap *Supercond. Sci. Technol.* **30** 123002
[12] Schmidt W, Gamble B, Kraemer H-P, Madura D, Otto A and Romanosky W 2009 Design and test of current limiting modules using YBCO-coated conductors *Supercond. Sci. Technol.* **23** 014024
[13] Búran M, Vojenčiak M, Mošať M, Ghabeli A, Solovyov M, Pekarčíková M, Kopera Ľ and Gömöry F 2019 Impact of a REBCO coated conductor stabilization layer on the fault current limiting functionality *Supercond. Sci. Technol.* **32** 95008

[14] Dai S *et al* 2019 Development and test of a 220 kV/1.5 kA resistive type superconducting fault current limiter *Phys. C Supercond. its Appl.* **565** 1253501

[15] Hahn S *et al* 2019 45.5-Tesla direct-current magnetic field generated with a high-temperature superconducting magnet *Nature* **570** 496–9

[16] Wimbush S C and Strickland N M 2017 A public database of high-temperature superconductor critical current data *IEEE Trans. Appl. Supercond.* **27** 8000105

[17] Strickland N M and Wimbush S C 2017 The magnetic-field dependence of critical current: what we really need to know *IEEE Trans. Appl. Supercond.* **27** 8000505

[18] Kubiczek K, Grilli F, Kario A, Godfrin A, Zermeño V M R, Stępień M and Kampik M 2019 Length uniformity of the angular dependences of Ic and n of commercial REBCO tapes with artificial pinning at 77 K *IEEE Trans. Appl. Supercond.* **29** 8000309

[19] Ainslie M D, Bumby C W, Jiang Z, Toyomoto R and Amemiya N 2018 Numerical modelling of dynamic resistance in high-temperature superconducting coated-conductor wires *Supercond. Sci. Technol.* **31** 074003

[20] Zhang M, Kvitkovic J, Kim C H, Pamidi S V and Combs T A 2013 Study of 2G high temperature superconducting coils: Influence of anisotropic characteristics *J. Appl. Phys.* **114** 043901

[21] Hong Z, Li W, Chen Y, Gömöry F, Frolek L, Zhang M and Sheng J 2018 Design optimization of superconducting coils based on asymmetrical characteristics of REBCO tapes *Phys. C Supercond. its Appl.* **550** 74–7

[22] Jiang Z, Endo N, Wimbush S C, Brooks J, Song W, Badcock R A, Miyagi D and Tsuda M 2019 Exploiting asymmetric wire critical current for the reduction of AC loss in hts coil windings *J. Phys. Commun.* **3** 095017

[23] Gömöry F, Šouc J, Adámek M, Ghabeli A, Solovyov M and Vojenčiak M 2019 Impact of critical current fluctuations on the performance of a coated conductor tape *Supercond. Sci. Technol.* **32** 124001

[24] Pardo E, Staines M, Jiang Z and Glasson N 2015 AC loss modelling and measurement of superconducting transformers with coated-conductor Roebel-cable in low-voltage winding *Supercond. Sci. Technol.* **28** 114008

[25] Goldacker W, Grilli F, Pardo E, Kario A, Schlachter S I and Vojenčiak M 2014 Roebel cables from REBCO coated conductors: a one-century-old concept for the superconductivity of the future *Supercond. Sci. Technol.* **27** 093001

[26] Long N J, Badcock R A, Hamilton K, Wright A, Jiang Z and Lakshmi L S 2010 Development of YBCO Roebel cables for high current transport and low AC loss applications *J. Phys. Conf. Ser.* **234** 022021

[27] Song W, Jiang Z, Zhang X, Staines M, Badcock R A, Fang J, Sogabe Y and Amemiya N 2018 AC loss simulation in a HTS 3-Phase 1 MVA transformer using H formulation *Cryogenics (Guildf).* **94** 14–21

[28] Hong Z, Campbell A M and Coombs T A 2006 Numerical solution of critical state in superconductivity by finite element software *Supercond. Sci. Technol.* **19** 1246–52

[29] Zermeno V M R, Abrahamsen A B, Mijatovic N, Jensen B B and Sørensen M P 2013 Calculation of alternating current losses in stacks and coils made of second-generation high temperature superconducting tapes for large scale applications *J. Appl. Phys.* **114** 173901

[30] Jiang Z *et al* 2010 Transport AC loss characteristics of a nine strand YBCO Roebel cable *Supercond. Sci. Technol.* **23** 025028

[31] Terzieva S, Vojenčiak M, Pardo E, Grilli F, Drechsler A, Kling A, Kudymow A, Gömöry F and Goldacker W 2010 Transport and magnetization ac losses of ROEBEL assembled coated conductor cables: measurements and calculations *Supercond. Sci. Technol.* **23** 014023

[32] Amemiya N, Tsukamoto T, Nii M, Komeda T, Nakamura T and Jiang Z 2014 Alternating current loss characteristics of a Roebel cable consisting of coated conductors and a three-dimensional structure *Supercond. Sci. Technol.* **27** 035007

[33] Grilli F and Zermeño V M R 2017 Effect of tape's Ic inhomogeneity and strand misalignment on the transport capacity of roebel cables *IEEE Trans. Appl. Supercond.* **27** 6603605

[34] Rodriguez-Zermeno V M, Mijatovic N, Traeholt C, Zirngibl T, Seiler E, Abrahamsen A B, Pedersen N F and Sorensen M P 2011 Towards faster FEM simulation of thin film superconductors: a multiscale approach *IEEE Trans. Appl. Supercond.* **21** 3273–6

[35] Hu D, Ainslie M D, Raine M J, Hampshire D P and Zou J 2016 Modeling and comparison of in-field critical current density anisotropy in high-temperature superconducting (HTS) coated conductors *IEEE Trans. Appl. Supercond.* **26** 6600906

[36] Jiang Z, Long N J, Staines M, Badcock R A, Bumby C W, Buckley R G and Amemiya N 2016 AC loss measurements in HTS coil assemblies with hybrid coil structures *Supercond. Sci. Technol.* **29** 095011

[37] Brandt E H and Indenbom M 1993 Type-II-superconductor strip with current in a perpendicular magnetic field *Phy. Rev.* B **48** 12893–906

[38] Jiang Z, Toyomoto R, Amemiya N, Zhang X and Bumby C W 2017 Dynamic resistance of a high-Tc coated conductor wire in a perpendicular magnetic field at 77 K *Supercond. Sci. Technol.* **30** 03LT01

[39] You S, Staines M, Sidorov G, Miyagi D, Badcock R A, Long N J and Jiang Z 2020 AC loss measurement and simulation in a REBCO coil assembly utilising low-loss magnetic flux diverters *Supercond. Sci. Technol.* **33** 115011

[40] Song W, Jiang Z, Staines M, Wimbush S, Badcock R and Fang J 2020 AC loss calculation on a 6.5 MVA/25 kV HTS traction transformer with hybrid winding structure *IEEE Trans. Appl. Supercond.* **30** 5500405